ON THE POROMECHANICAL MODELLING AND INTERPRETATION OF FIELD VANE TEST

Mateus Forcelini

forcelini.mateus@gmail.com

Department of Civil Engineering, Federal University of Rio Grande do Sul
Av. Osvaldo Aranha 99, 3rd floor, CEP 90035-190, Porto Alegre, RS, Brazil

Samir Maghous

samir.maghous@ufrgs.br

Department of Civil Engineering, Federal University of Rio Grande do Sul
Av. Osvaldo Aranha 99, 3rd floor, CEP 90035-190, Porto Alegre, RS, Brazil

Gracieli Dienstmann

g.dienstmann@gmail.com

Department of Civil Engineering, Federal University of Santa Catarina
R. João Pio Duarte da Silva 205, CEP 88040-900, Florianópolis, SC, Brazil

Felipe Schaedler de Almeida

felipe.almeida@ufrgs.br

Department of Civil Engineering, Federal University of Rio Grande do Sul
Av. Osvaldo Aranha 99, 3rd floor, CEP 90035-190, Porto Alegre, RS, Brazil

Fernando Schnaid

fschnaid@gmail.com

Department of Civil Engineering, Federal University of Rio Grande do Sul
Av. Osvaldo Aranha 99, 3rd floor, CEP 90035-190, Porto Alegre, RS, Brazil

Abstract. The field vane test is probably the most used apparatus for evaluation of undrained shear strength of clay deposits. Although being designed for low permeability soils, its application in intermediate permeability materials can also be found in geotechnical investigation practice. Since the standard rate of shearing may not ensure undrained conditions in those cases, attention must be paid to partial drainage effects in the soil surrounding the vane, leading to an increase in the soil resistance and an erroneous estimation of the undrained strength. This paper aims to investigate the drainage effects by means of a nonlinear poroelastic model, conceived to capture the transient flow effects in the medium surrounding a rotating cylinder, which can be viewed as a simplified conceptual model for the vane geometry. The model relies on a nonlinear poroelastic stress-strain analysis addressed by the Biot's poroelasticity framework, where closed-form expressions for pore pressure distribution were derived while stress and displacements are computed numerically through a finite difference scheme. The nonlinear poroelastic model is briefly presented and validated through experimental results in low permeability soils. A parametrical analysis is then conducted to evaluate the response of theoretical materials varying strength, stiffness and influence radius size. Finally, the numerical model is applied to the interpretation of experimental data in zinc mining tailings, viewed as intermediate permeability materials. It has been shown that the proposed poroelastic model is a good tool in evaluating the drainage effects in vane tests, allowing for the identification of test patterns that ensures the desired drainage behavior.

Keywords: Field vane test, Porous medium, Nonlinear poroelasticity, Rate effects, Transient flow.

1   Introduction

In geotechnical investigation practice, the field vane test has been the most commonly used tool for in-situ evaluation of the undrained shear strength S_u of clays, mainly as a result of its simplicity, low cost and fast execution (Flaate [1]; Chandler [2]; Roy and Leblanc [3]). Even though it can also be applied to coarser grained materials, attention must be paid to the possibility of drainage in the soil surrounding the vane, which is likely to occur in transient soils (intermediate permeability ranging from $10^{-5} < k < 10^{-8}$ m/s) such as silts. This phenomenon leads to an increase in the effective stresses around the vane and thus an increase in the soil shear strength, inducing an overestimated undrained resistance by the classical interpretation of the test.

The literature demonstrates that the standard rate of vane rotation (0.1 deg/s), which ensures undrained conditions of shearing in low permeability materials, may not be applicable to estimate the undrained resistance of silts (Bedin [4]; Schnaid [5]; Gauer [6]; Hlenka [7]; Dienstmann [8]; Gauer [9]; Fayolle [10]). One particular application is the interpretation of field vane tests conducted in mining tailings that, due to its hydraulic disposal process, often produces silt-particle materials. Therefore, changing the rate of vane rotation to control the drainage conditions developed during the test may be a key element to obtain reliable constitutive parameters in undrained conditions of these soils.

To capture these transient flow effects, a simplified model for the poromechanical analysis of the consolidation induced by an infinitely long rigid cylinder rotating within a porous medium was formulated by Dienstmann et al. [11], with the rigid cylinder being a conceptual simplified geometry of the vane test. The model relies on the Biot's poroelasticity framework, contemplating a nonlinear poroelastic stress-strain analysis of porous media subjected to shear and compressive stresses, allowing for the analysis of the coupled deformation-diffusion process.

In order to assess the drainage effects, drainage curves are extensively used to represent the drainage degree U^* as a function of a non-dimensional velocity (Blight [12]; Randolph and Hope [13]). This approach was initially adopted by Blight [12] in order to establish limits of velocity that ensures completely undrained conditions of shearing in silty soils and mining wastes.

The present work aims to evaluate how the drainage conditions of intermediate permeability soils are affected by different rates of rotation via the above-mentioned model. Firstly, the poromechanical model is validated for application to vane shear test analysis through experimental data in low permeability soils (clayey-grained) subjected to different rates of shearing. On a subsequent stage, a parametrical analysis is performed to evaluate the poromechanical response of theoretical materials varying internal friction angles, initial stiffness, and radius of influence. Finally, the model predictions are attained for field vane tests carried out in a zinc mining tailing dam, which demonstrates that the standard velocity is not suitable to reach undrained conditions in intermediate permeability material, and allows for the identification of test patterns that ensures the desired drainage behavior.

2   Framework of analysis

The study is based upon the simplified poromechanical model conceived by Dienstmann et al. [11] and adopted for the analysis of consolidation induced by the rotation of a rigid cylinder embedded within an isotropic poroelastic medium of infinite extent. The analysis is based on the assumption of plane strain conditions, restricting the displacements and flow to a two-dimensional setting. The consolidation problem starts from an initial poromechanical state where a prescribed rotational displacement $\alpha(t)R\underline{e}_\theta$ is imposed at the cylinder wall $r = R$, where R is the cylinder radius. Due to the consolidation, the soil around the cylinder is subjected to a combination of radial and rotational displacements (ξ_r and ξ_θ, respectively), as can be seen by Figure 1.

CILAMCE 2019

Proceedings of the XLIbero-LatinAmerican Congress on Computational Methods in Engineering, ABMEC,
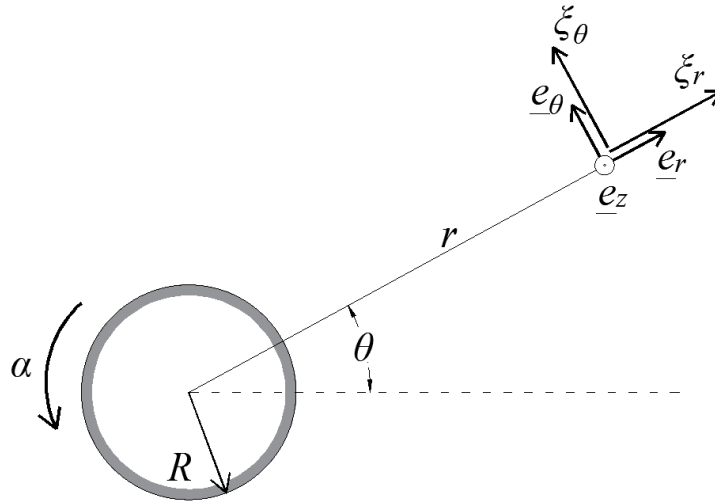Natal/RN, Brazil, November 11-14, 2019

Figure 1. Geometry model and loading mode for consolidation
around an infinite rotating cylinder.

The soil surrounding the cylinder is modeled as a fully saturated poroelastic material undergoing infinitesimal strains, where the interface soil/rigid cylinder is assumed to have perfect bonding at all stages. On a macroscopic scale, the porous medium is the superimposition of two continua: the skeleton continuum (matrix) and the fluid continuum, so that any infinitesimal volume can be treated as the superimposition of two material particles. The classical soil mechanics sign convention with compressive stresses and strains counted as positive will be adopted throughout the paper.

2.1 Nonlinear poroelastic state equations

The resolution of a problem in poroelasticity is similar to conventional elasticity, yet, the interaction between the solid matrix and the pore fluid should be taken into account. The poroelastic state equations for a saturated isotropic material can be expressed within the framework of infinitesimal strain as (Coussy [14]; Dormieux et al. [15]):

$$\Delta \underline{\underline{\sigma}} = \lambda \operatorname{tr} \underline{\underline{\varepsilon}} \underline{\underline{1}} + 2G \underline{\underline{\varepsilon}} - b \Delta p \underline{\underline{1}} \tag{1}$$

$$\Delta \Phi = -b \operatorname{tr} \underline{\underline{\varepsilon}} + \frac{1}{M} \Delta p \tag{2}$$

where λ and G are the Lamé constants for the skeleton phase, while b and M denotes the Biot coefficient and Biot modulus, respectively. The first state equation relates the stress change $\Delta \underline{\underline{\sigma}} = \underline{\underline{\sigma}} - \underline{\underline{\sigma}}_0$ to the skeleton infinitesimal strain $\underline{\underline{\varepsilon}}$ and the pore-fluid pressure change $\Delta p = p - p_0$, while the second state equation relates the lagrangian porosity change $\Delta \Phi = \Phi - \Phi_0$ to the volumetric strains and the pore-fluid pressure change. The Biot parameters are related to the skeleton bulk modulus K and the solid grain bulk modulus K_s through:

$$b = 1 - \frac{K}{K_s} \qquad ; \qquad \frac{1}{M} = \frac{b - \Phi}{K_s} \tag{3}$$

According to the approach contrived by Dienstmann et al. [11], the analysis is controlled by the nonlinear behavior of the porous medium surrounding the rotating cylinder. The idea of this feature is to model a fictitious nonlinear poroelastic behavior that asymptotically meets the plastic yield criteria of the material. This condition is formulated as a function of Terzaghi effective stress by:

$$\lim_{\varepsilon_d / \varepsilon_{ref} \to \infty} F\left(\underline{\underline{\sigma}}' = \underline{\underline{\sigma}} - p\underline{\underline{1}}\right) = 0 \tag{4}$$

where ε_d is the equivalent deviatoric stress and ε_{ref} is a reference strain whose magnitude may be evaluated from the elastic limit shear strain. In all the analysis presented through the paper, a Drucker-Prager yield condition is adopted for the asymptotical behavior described by Eq. (4). This yield criterion may be expressed by:

$$F\left(\underline{\underline{\sigma}}'\right) = \sigma_d - T\left(h + \sigma_m'\right) \le 0 \tag{5}$$

where σ_d and σ_m' denotes the equivalent deviatoric stress and the mean effective stress, respectively, while h and T are material parameters that refer to the material's friction coefficient and tensile strength following the Drucker-Prager criterion. Throughout the paper, these parameters will be computed from the inscribed Mohr-Coulomb yield surface with reference to the Drucker-Prager cone.

Following the condition expressed by Eq. (4) one way to achieve the desired behavior is to consider in the poroelastic medium a nonlinear secant shear modulus that evolves with the strain levels, while the bulk modulus K is held constant (Lemarchand et al. [16]; Maghous et al. [17]; Dienstmann et al. [11]). The asymptotic behavior for secant shear modulus could then be expressed as:

$$G\left(\varepsilon_d, \varepsilon_v, p\right) \approx \frac{T}{2\varepsilon_d}\left[h + K\varepsilon_v + \sigma_{0m}' - \left(1 - b\right)\Delta p\right] \qquad \text{when } \varepsilon_d / \varepsilon_{ref} \gg 1 \tag{6}$$

where $\varepsilon_v = \text{tr}\,\underline{\underline{\varepsilon}}$ represents the skeleton volumetric strain and $\sigma_{0m}' = \text{tr}\,\underline{\underline{\sigma}}_0' / 3$ is the mean initial effective stress. In order to satisfy equation (6), the approach proposed by Maghous et al. [17] is adopted in the context of poroelasticity through the following law for the secant shear modulus:

$$G\left(\varepsilon_d, \varepsilon_v, p\right) = \frac{T}{2\varepsilon_d}\left[h + K\varepsilon_v + \sigma_{0m}' - \left(1 - b\right)\Delta p\right] \times \frac{1 / \varepsilon_{ref}}{1 + \varepsilon_d / \varepsilon_{ref}} \tag{7}$$

This nonlinear asymptotic behavior adopted is presented in Figure 2, remarking that $\sigma_d = 2G\varepsilon_d$. It should be noted that both the Biot coefficient b and Biot modulus M are constant material parameters since the skeleton bulk modulus is assumed constant during the shear process. The fictitious poroelastic behavior presented involves a secant shear modulus that depends on the skeleton strains and pore-fluid pressure. However, it should be pointed out that this shear modulus is referring to a fictitious constitutive parameter, and not to a material property, which stems from a mathematical equivalence between elastoplastic and related non-linear elastic response.
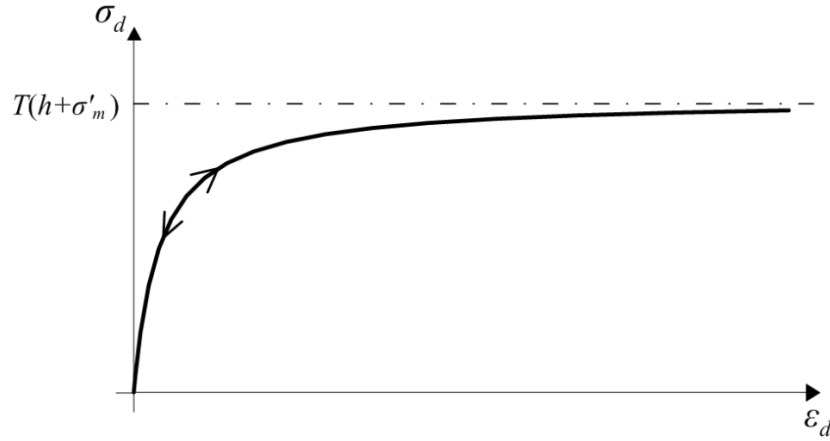
Figure 2. Schematic representation of the nonlinear elastic behavior associated with the Drucker-Prager yield criterion

2.2 Governing equations for the consolidation problem

Accordingly to the continuum mechanics, the solution that describes the stress field and the pore-fluid pressure generated during the cylinder rotation has to obey the local equilibrium equation, expressed as:

$$\text{div}\,\Delta\underline{\underline{\sigma}} = 0 \tag{8}$$

The solution is then investigated through a displacement approach, where the displacement field induced by the cylinder rotation can be stated as a combination of radial functions:

$$\underline{\xi} = f(r)\underline{e}_r + g(r)\underline{e}_\theta \tag{9}$$

where $\underline{\xi}$ is the displacement vector and the radial functions $f(r)$ and $g(r)$ represents, respectively, the rotational displacements due to cylinder rotation and the radial displacements induced by the pore-fluid pressure diffusion in the soil mass. The mechanical boundary conditions completing the displacement field are expressed as:

$$\underline{\xi} = \alpha R \underline{e}_\theta \quad \text{at } r = R \;\forall t \tag{10}$$

$$\underline{\xi} = 0 \quad \text{at } r = a \;\forall t \tag{11}$$

The first condition implies that a rotation angle α is imposed at the cylinder wall ($r = R$), while the second condition indicates that the displacement induced by the movement of the rigid cylinder is null at a distance $r = a > R$. The latter condition establishes the concept of a zone of influence, that is, a radial distance a in which the displacements and of skeleton particles as well as pore-fluid pressure change of the medium is no longer affected by the cylinder inclusion and rotation. The hydraulic boundary conditions of the problem are stated as:

$$u = u_{max} \text{ and } \frac{\partial u}{\partial r} = 0 \quad \text{at } r = R \tag{12}$$

$$u = 0 \text{ and } \frac{\partial u}{\partial r} = 0 \quad \text{at } r = a \tag{13}$$

Equation (12) declares that, at the interface soil/rigid cylinder, the excess pore pressure presents

its maximum value and its gradient is null, mathematically declaring the impermeability of the rigid cylinder. Whereas, Eq. (13) expresses that at the end of the influence zone, the excess pore pressure is null and no fluid flow occurs beyond this limit.

Combining the fluid mass balance, Darcy's law and the second poroelastic state equation (Eq. (2)), is possible to derive the following expression:

$$-b\frac{\partial \operatorname{tr} \underline{\underline{\varepsilon}}}{\partial t} + \frac{1}{M}\frac{\partial \Delta p}{\partial t} = k\nabla^2 u \qquad (14)$$

where k is the hydraulic conductivity of the porous medium, u is the pore-fluid pressure, t is the time and ∇^2 is the Laplacian operator. Combining Eqs. (8) and (1) is possible to obtain an expression derived from the Navier generalized equation (Dienstmann et al. [11]):

$$\left[K+\frac{4}{3}G\right]\nabla\left(\operatorname{tr}\underline{\underline{\varepsilon}}\right) + G\operatorname{rot}\left(\operatorname{rot}\underline{\xi}\right) + 2\nabla G \cdot \left(\underline{\underline{\varepsilon}} - \frac{1}{3}\operatorname{tr}\underline{\underline{\varepsilon}}\underline{\underline{1}}\right) = -b\nabla\left(\Delta p\right) \qquad (15)$$

Contrasting with the usual formulations developed in linear poroelasticity, the pore-fluid distribution is connected to the volumetric strains $\varepsilon_v = \operatorname{tr}\underline{\underline{\varepsilon}}$ as well as the deviatoric strain. This aspect stems from the shear modulus dependence law with respect to $\underline{\underline{\varepsilon}}$.

The coupled poromechanical problem concerning the consolidation induced by cylinder rotation is defined through Eqs. (8) and (15), together with the mechanical and hydraulic boundary conditions. In order to solve the model presented herein, a time-incremental procedure has been developed for Dienstmann et al. [11], where a specific iterative algorithm based on a finite difference scheme is implemented within each time step, allowing the assessment of semi-analytical solutions for stress, displacement, and pore-fluid pressure.

2.3 Distribution of initial excess pore-fluid pressure

One of the fundamental inputs of the model is the value and distribution of initial excess pore-fluid pressure $u_0(r) = u(r, t=0)$, prior to the cylinder rotation. This initial excess pore pressure is generated due to the particle displacement during the vane (or another probe) insertion in the porous medium. In literature, field measurement of $u_0(r)$ in the vicinity of rigid inclusions and their distribution in the soil mass are rarely reported, with the available data indicating that it exhibits a maximum value $u_{0,max}$ close to the inclusion wall ($r = R$) and decreases radially, becoming negligibly small at a certain radius of influence $r = a$ (Lo and Stermac [18]; Morris and Williams [19]; Randolph and Wroth [20]; Chai et al. [21]).

In order to fit experimental data, some mathematical expressions have been proposed in the literature for the initial excess pore pressure distribution (e.g. linear, parabolic, logarithmic…). Yet, it can be easily verified that none of the above complies with the following boundary conditions:

$$\begin{cases} \dfrac{\partial u_0}{\partial r} = 0 & \text{at } r = R \\[2mm] \dfrac{\partial u_0}{\partial r} = 0 & \text{at } r = a \end{cases} \qquad (16)$$

which physically express the cylinder wall impermeability condition and the that there is no fluid flow beyond the radius of influence. Based on these considerations, the following expression is proposed for initial excess pore pressure:

$$u_0(r) = u_{0,max}\frac{\mathscr{F}(r)}{\mathscr{F}(R)} \quad \text{with} \quad \mathscr{F}(r) = A\left(1 + \frac{r}{R} - \frac{a}{r} - \frac{a}{R}\right) + \frac{a}{R}\ln\left(\frac{a}{r}\right) \qquad (17)$$

where the dimensionless parameter A is computed as $A = \dfrac{a/R}{\left(1 + a/R\right)}$. Equation (17) is a combination of linear, hyperbolic and logarithmic terms, extending the formulation proposed by Dienstmann et al. [11]. A demonstration of Eq. (17) applicability is illustrated in Figure 3 comparing it to the experimental data available. In this plot, Lo and Stermac [18] data were obtained during driving piles on silty clays and Chai et al. [21] values were obtained after a mini piezocone insertion on a calibration chamber filled with sand. It can be seen that for a radius of influence $a = 35R$ the proposed distribution shows reasonable agreement with the literature data, although it should be noted that this relatively high value of the ratio a/R is rather representative of pile driving mechanisms, which resemble cavity expansion process, diverging from the insertion of a standard four-bladed vane. Hence, the distribution presented by Eq. (17) will be adopted throughout this paper.
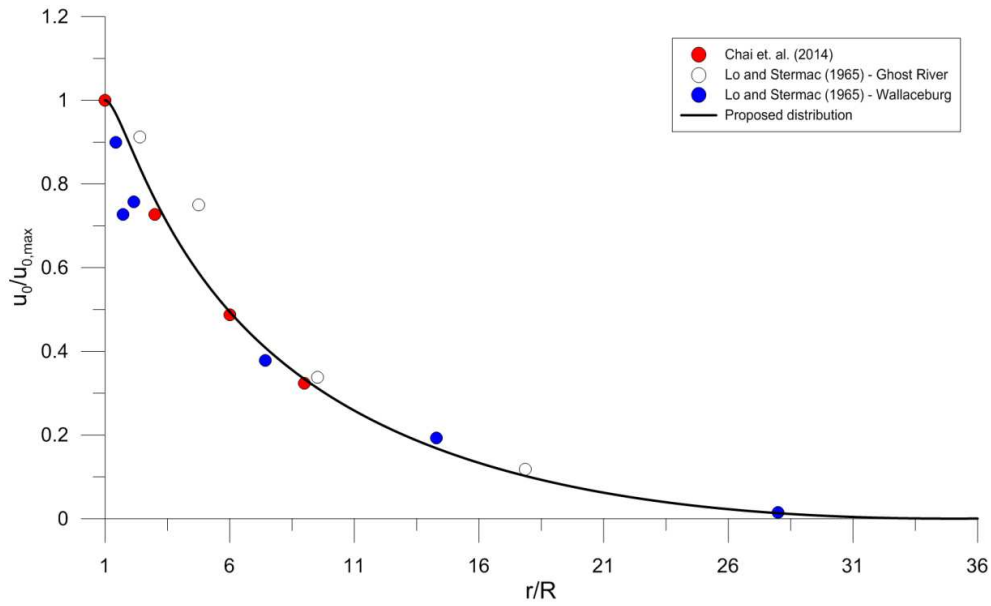

Figure 3. Initial excess pore-fluid pressure distribution versus distance to the cylinder axis.

According to Dienstmann et al. [11], the value of $u_{0,max}$ can be computed correlating the rigid cylinder insertion into the soil with a cavity expansion problem, where typical solutions derived in this context suggests that $u_{0,max}$ can be evaluated from the stress paths develops in undrained triaxial tests carried out until the ultimate state is attained (Vésic [22]). Thus, the maximum initial excess pore pressure can be estimated for normally consolidated soils as:

$$u_{0,max} = \frac{p_{c0}}{2}\left(1 + M_{cs}\right) \qquad (18)$$

where p_{c0} is the initial consolidation pressure and M_{cs} refers to the slope of the critical state line. It should be regarded that Eq. (17) assumes that no pore-fluid pressure dissipation occurs prior to the vane rotation, which implicitly entails that the cylinder installation is fast and the elapsed time between installation and rotation is short enough for the pore pressure does not dissipate. In addition, due to the absence of knowledge about the initial stress distribution in the soil mass immediately after the cylinder insertion, a simplified isotropic initial stress field will be adopted in the numerical analysis.

3   Model Validation

Most of previously reported data related to vane rate effects attempted to evaluate the impact of

velocities higher than the standard (i.e. $\omega > 0.1$ deg/s), thus observing viscous effects on the measured resistance (e.g. Perlow and Richards [23]; Torstensson [24], Biscontin and Pestana [25]; Schlue et al. [26]), which are not the subject of the present paper, since the constitutive laws adopted in the poroelastic model does not account for these effects. Therefore, the model is restricted to applications where partial drainage can be observed, usually for velocities below 0.1 deg/s in low permeability materials.

Model predictions presented herein were compared to the experimental results presented by Roy and Leblanc [3] on silty-clays, a low permeability material, in order to compare the resistance developed during shearing and obtain the drainage conditions for the field data, thereby validating the poroelastic model application. The clay deposits under study present low compressibility and a small porosity for its granulometry range, with a void ratio e smaller than 1.6 for all the samples taken.

The set of vane tests performed by Roy and Leblanc [3] were carried out in two distinct sites in Canada, namely Saint-Alban and Saint-Louis de Bonsecours. The authors adopted five distinct rotation rates of 0.014, 0.042, 0.084, 0.22 and 1.9 deg/s, using a standard vane apparatus ($D = 65$ mm and $H = 130$ mm) at a depth of 12 meters. According to the authors, undrained conditions were achieved for $\omega = 0.22$ deg/s, since the smallest torque was recorded in this condition. For lower shear rates, the resistance increased significantly due to partial drainage effects, while for shear rates above 0.22 deg/s, the torque measured also presented an increase related to rheological effects.

In order to conduct the numerical simulations, the constitutive parameters adopted for the porous medium were evaluated through empirical correlations, since the author's data lack of more realistic values. The small strain shear modulus G_0 was estimated from the correlation proposed by Jamiolkowsky et al. [27], while the initial value of the Poisson coefficient was adopted as $\nu_0 = 0.2$. A friction angle φ equal to 26° was assumed, classically representative of soft clay deposits, whereas the magnitude of the cohesion c' was calibrated from the lowest torque measured, considered in undrained conditions.

A grain bulk modulus $K_s = 10$ GPa was adopted, as recommended by Djeran-Maigre and Gasc-Barbier [28] for the computation of Biot coefficient and Modulus. The initial stress state was considered isotropic and computed for the depth of 12 meters, while the radius of influence was calibrated by several numerical simulations as $a = 5R$. A hydraulic conductivity $k = 10^{-9}$ m/s was assumed, considered to be in the range of low permeability soils (Schnaid [5]). The parameters adopted in the numerical simulations for Roy and Leblanc [3] data are summarized in Table 1.

Table 1. Constitutive parameters adopted in Roy and Leblanc [3] simulations.

Parameter	Value	
	Saint-Alban	Saint-Louis de Bonsecours
φ (deg)	26	26
c' (kPa)	11.70	11.90
$u_{0,max}$ (kPa)	64.04	68.85
G_0 (MPa)	45.85	24.39
ν_0	0.2	0.2
b	0.998	0.999
M (GPa)	4.17	3.46
ε_{ref}	$1.269 \cdot 10^{-3}$	$2.534 \cdot 10^{-3}$
k (m/s)	10^{-9}	10^{-9}
$\sigma_0' = \sigma_{v0}' = \sigma_{h0}'$ (kPa)	89.33	96
e	1.00	1.59
a/R	5	5

The results of drainage degree $U^* = 1 - \dfrac{u}{u_{0,max}}$ obtained through the model simulation are presented as a function of the rotational velocity normalized by the hydraulic conductivity v/k for both sites under study in Figure 4(a), with both points and full lines computed from the poroelastic model, since the standard vane apparatus does not allow for pore pressure measures. As can be seen, the behavior transition from drained to partially drained are observed for v/k close to 10^2, while the transition for partially drained to undrained for $v/k \approx 10^4$. The numerical results also sustain that the standard vane velocity is suitable to achieve undrained conditions ($U^* < 5\%$) in this low permeability material.
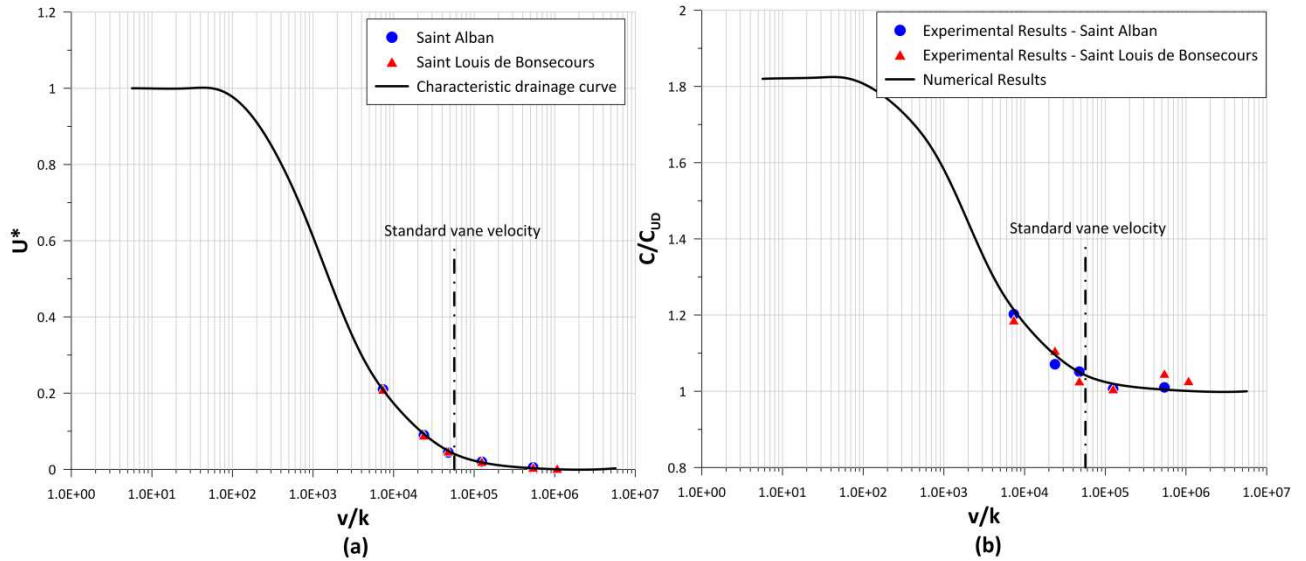

Figure 4. Variation of (a) normalized torque and (b) drainage degree with v/k (experimental data after Roy and Leblanc [3]).

Figure 4(b) presents the normalized torque C/C_{UD} as a function of the v/k, where C_{UD} corresponds to the torque at undrained conditions, with the line obtained numerically and the points experimentally. It can be seen that the numerical predictions were able to capture the trend of increasing resistance with a reduction in the shear rate of the experimental data. Although the velocities required to achieve fully drained conditions may be too slow to be adopted in field vane tests, the model predicts a drained torque value C_{DR} approximately 1.85 times higher than the undrained one.

It should be pointed out that even though the initial pore pressure distribution was validated for $a = 35R$, the adoption of a smaller radius of influences seems reasonable for the problem of a vane inclusion in the soil mass, since cylindrical inclusions (e.g. driven piles and piezocones) disturb a larger soil mass than the four-bladed geometry of the field vane, as its cross-sectional area corresponds to approximately 7.5% of a circle are of the same diameter.

4   Parametric Analysis

One of the main advantages of preserving semi-analytical treatment of the poromechanics governing equations in the simplified poroelastic model is to allow for intensive parametric studies. In this sense, a parametrical analysis concerning the main parameters of the porous medium is conducted, in order to assess the effects of the extent of influence zone, soil stiffness and strength in the observed torque and drainage degree.

4.1 Impact of influence radius size

The radius of influence is a fundamental input for the numerical model since it determines the distance affected by the initial excess pore pressure induced due to the cylinder insertion. Thus, numerical simulations with the ratio $a/R \in \{5,10,15\}$ were conducted with a rigid cylinder of $R = 32.5$ mm, adopting a theoretical material with $\varphi = 25°$, $c' = 1$ kPa, $G_0 = 25$ MPa, $\nu_0 = 0.2$, $e = 1$ and hydraulic conductivity of $k = 10^{-7}$ m/s, typical of intermediate permeability soils.

The results for drainage degree and normalized torque curves obtained through the numerical model are presented in Figure 5(a) and (b), respectively. As can be seen, the radius of influence size affects both the drainage and torque curves. In general, undrained condition is achieved for higher velocities in materials with a smaller influence radius, i.e., the dissipation occurs faster for lower values of a/R. It can also be noted that the standard rate of vane rotation ($\omega = 0.1$ deg/s) is not sufficiently fast to achieve undrained conditions in this intermediate permeability material, irrespective to the radius considered.
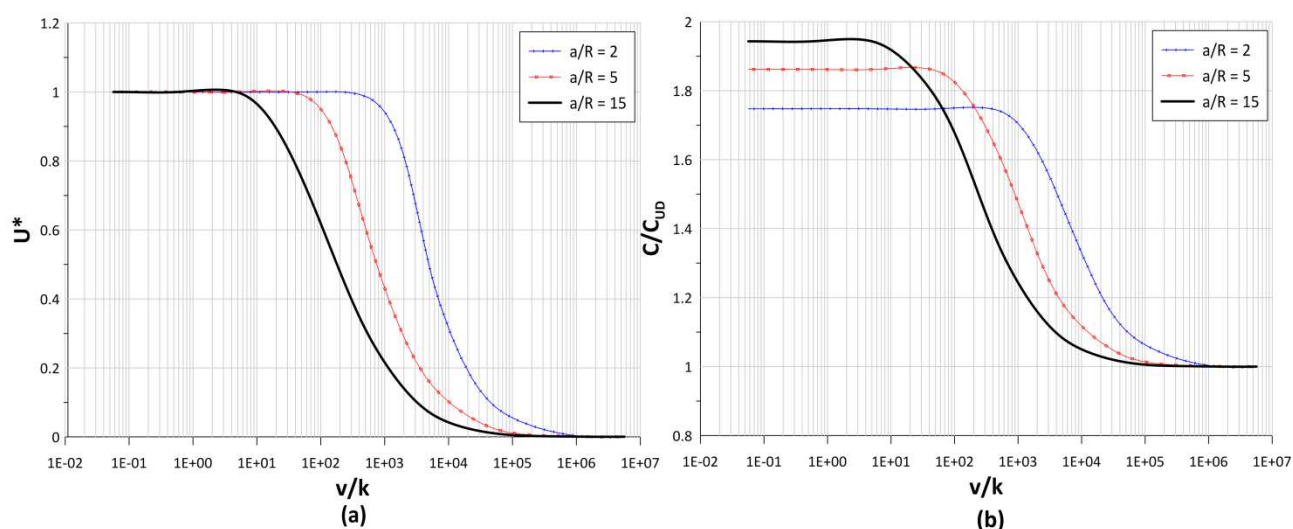

Figure 5. (a) Drainage degree and (b) normalized torque curves for materials varying the radius of influence size.

As can be seen by the torque curves in Figure 5(b), the ratio between drained and undrained torques increases from 1.75 for $a/R = 2$ to 1.97 for $a/R = 15$. Additional simulations not presented herein demonstrate that an asymptotic value is achieved for values of a/R higher than 15, demonstrating that the influence radius size has little effects on changes in torque attributed to drainage effects.

4.2 Influence of initial shear modulus G_0

The influence of the initial stiffness of the soil was evaluated through a series of numerical simulation varying the initial shear modulus in the range of 5 to 100 MPa within a theoretical material with $\varphi = 25°$, $c' = 1$ kPa, $\nu_0 = 0.2$, $e = 1$, $k = 10^{-7}$ m/s and a fixed influence radius of $a/R = 5$. The results are presented in Figure 6, where it can be seen that both the drainage degree and mobilized torque are little affected by the magnitude of G_0. Again it can be seen as expected that the standard vane velocity does not ensure undrained condition for the materials considered.
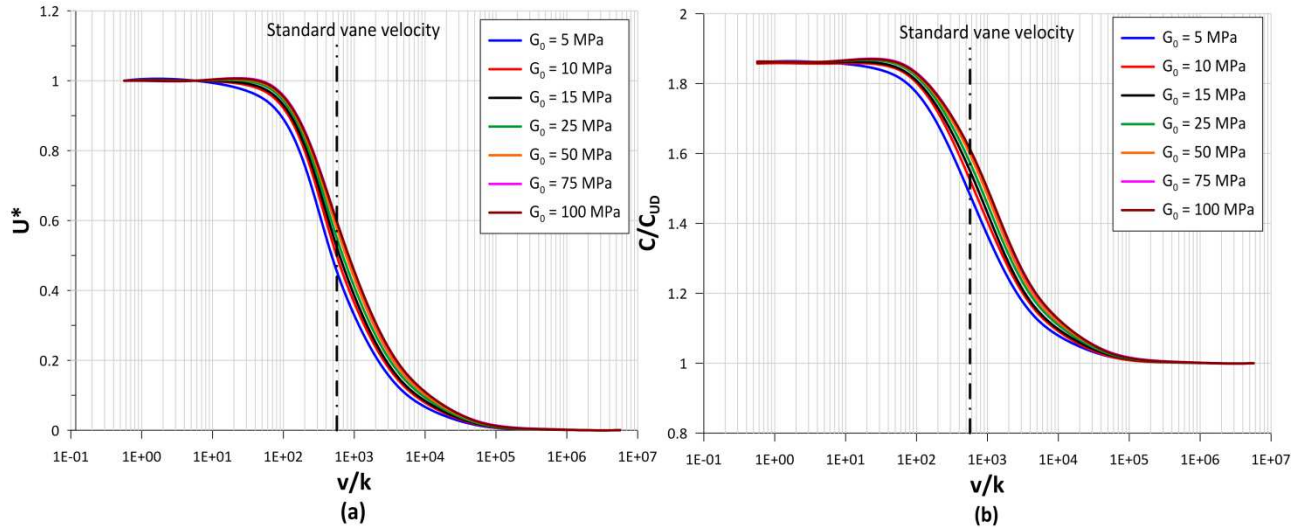
Figure 6. (a) Drainage degree and (b) normalized torque curves for materials varying initial shear modulus.

4.3 Influence of friction angle φ

The influence of material's resistance is evaluated through a parametrical analysis of the soil friction angle. Thus, simulations on a theoretical material with $\varphi \in \{20, 25, 35\}$ in a material with fixed properties $c' = 1$ kPa, $G_0 = 25$ MPa, $\nu_0 = 0.2$, $e = 1$, $k = 10^{-7}$ m/s and $a/R = 5$. Figure 7 presents the results obtained for drainage degree and normalized torque. It can be seen by Figure 7(a) the material's resistance presents little influence on the characteristic drainage curves, with stronger materials dissipating faster the pore pressure. It is observed that the velocity required to produce undrained shearing is of about 100 times faster than the standard vane rotation.
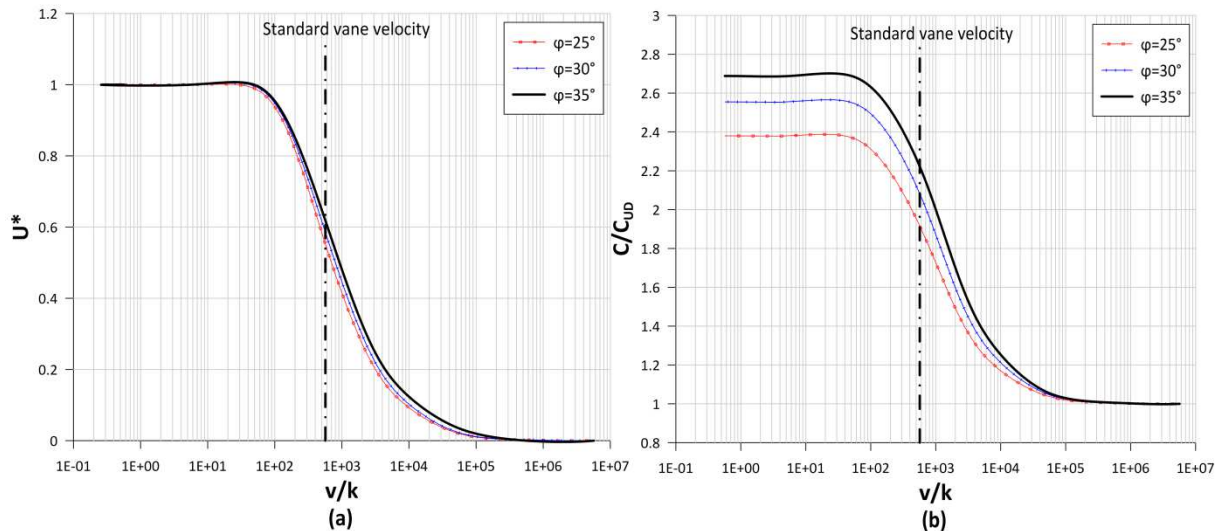

Figure 7. Effects of the soil friction angle on the (a) characteristic drainage curves and (b) normalized torque.

From Figure 7(b) it is evident that the friction angle affects the ratio between drained to undrained torques, mainly due to the fact that volumetric strains are induced by vane rotation in the drained regime, which affect the local soil shear strength and thus the mobilized torque at drained conditions (Dienstmann et al. [11]). Figure 8 presents the results of the normalized torque C_{DR} / C_{UD} as a function of $\tan \varphi$ for φ values ranging from 5 to 45° and initial stresses of 150, 300 and 500 kPa. As

is observed, this ratio is not too sensible of the initial effective stress, being the results lower than 3 for all cases observed. For the analysis developed, this ratio can be approximated in the interval proposed by the following function:

$$C_{DR}/C_{UD} = \frac{3}{2}\left[1+\tanh\left(r_\varphi\right)\right] \quad \text{with } r_\varphi = \frac{7}{4}\tan\varphi \qquad (19)$$

Which can be used as a guideline to estimate the maximum error in a field vane test in the case that the test is performed under fully drained conditions.
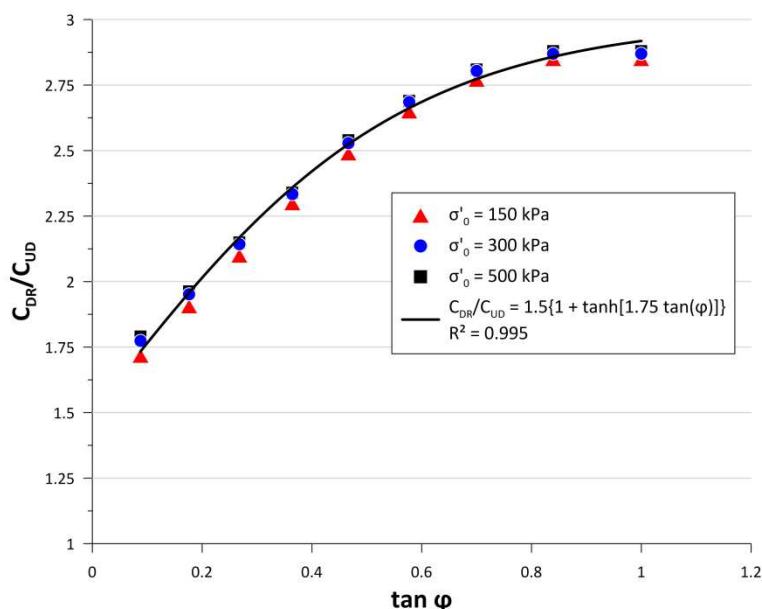

Figure 8. Drained to undrained torque ratio as a function of the friction angle.

5   Application of the poroelastic model to field vane test in zinc mining tailings

An interest case study is the interpretation of field vane tests conducted in silty soils such as mining tailings. This material usually presents an intermediate permeability, a high degree of heterogeneity and silty particle size as a consequence of its hydraulic disposal process, with often leads to partially drained behavior during vane tests conducted at the standard velocity. These behavioral characteristics were observed by Hlenka [7] in zinc mining tailings from a deposit in Juiz de Fora, Minas Gerais, Brazil.

In his work, Hlenka [7] performed a series of vane tests on a zinc tailing dam, adopting three different rotation rates ($\omega = 0.017$, 0.1 and 1.0 deg/s) in three different clusters (PZC01, PZC02, and PZC03) at three depths (2, 4 and 6 meters). Laboratory characterization of the material shows that the tailing is predominantly composed of silt particles (83% on average), presenting a high specific gravity ranging from 3.28 to 3.37 g/cm³. The soil also demonstrates high values of void ratio ($3.4 < e < 6.8$) as a result of its high moisture content ($90\% < w_n < 210\%$). According to the author results, the hydraulic conductivity k is equal to $2 \cdot 10^{-7}$ m/s, in the range of intermediate permeability soils.

In addition to the laboratory investigation, seismic piezocone tests (SCPTU) were conducted in all the clusters evaluated, allowing for direct assessment of G_0 values. The parameters adopted in the simulations are described in Table 2, where the values of friction angle were evaluated from cone tests whereas the values of c' were adjusted numerically following the procedure describe in section 3. The radius of influence a was considered as $5R$ following the calibration in clay materials since no other data provided could be used to estimate its magnitude.

Table 2. Parameters adopted for the Hlenka [7] material.

Parameter	PZC01			PZC02			PZC03		
	2 m	4 m	6 m	2 m	4 m	6 m	2 m	4 m	6 m
φ (deg)	31	31	31	32	32	32	35	35	35
c' (kPa)	0.40	0.60	2.00	2.31	4.42	9.63	4.40	4.86	11.17
$u_{0,max}$ (kPa)	3.29	6.60	10.75	4.08	8.82	13.46	2.75	6.60	11.24
G_0 (MPa)	6.08	3.26	4.08	3.14	3.45	2.46	7.71	11.15	12.24
v_0	0.2								
b	1.00	1.00	1.00	1.00	1.00	1.00	1.00	1.00	1.00
M (GPa)	12.6	10.3	9.88	11.08	9.98	10.38	10.28	11.58	8.31
k (m/s)	$2 \cdot 10^{-7}$								
σ'_0 (kPa)	4.46	8.96	14.59	5.52	11.92	18.2	3.68	8.84	15.05
e	6.91	4.93	4.63	5.58	4.71	5.02	4.93	5.98	3.50
a/R	5								

Figure 9 presents the model predictions together with the field vane test results for each cluster, where the symbols correspond to experimental data while the continuous lines to numerical predictions. It can be seen that despite some few points mainly at the depth of 6 meters, the proposed simulations reproduced the experimental results with reasonable agreement.

The complete characteristic drainage obtained by means of the poroelastic numerical simulations is presented in Figure 10(a). According to the results, the standard rate of rotation, equivalent to a normalized velocity of $v/k = 2.84 \cdot 10^2$ is not sufficiently fast to ensure undrained conditions of shearing. It can be seen that, due to the clusters heterogeneities, the angular velocity required to produce undrained behavior ranges from 0.6 to 5 deg/s, while drained conditions of shearing are expected for rotation velocities ranging from $8 \cdot 10^{-4}$ to 0.017 deg/s.
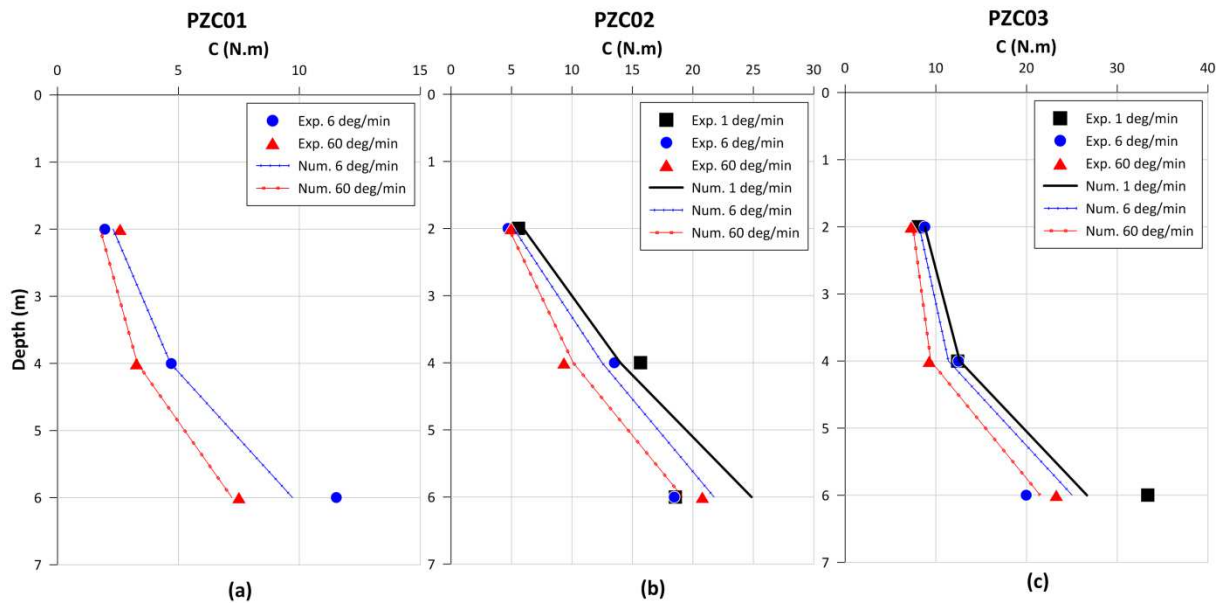

Figure 9. Numerical and experimental torque profiles at stations (a) PZC01, (b) PZC02 and (c) PZC03 (experimental data after Hlenka [3]).

The normalized torque curves obtained numerically are presented in Figure 10(b) as a function of v/k. Due to the heterogeneities mentioned above, distinct C/C_{UD} ratios are predicted for each cluster and depth, with the drained torque C_{DR} ranging from 1.23 to 2.24 times the undrained
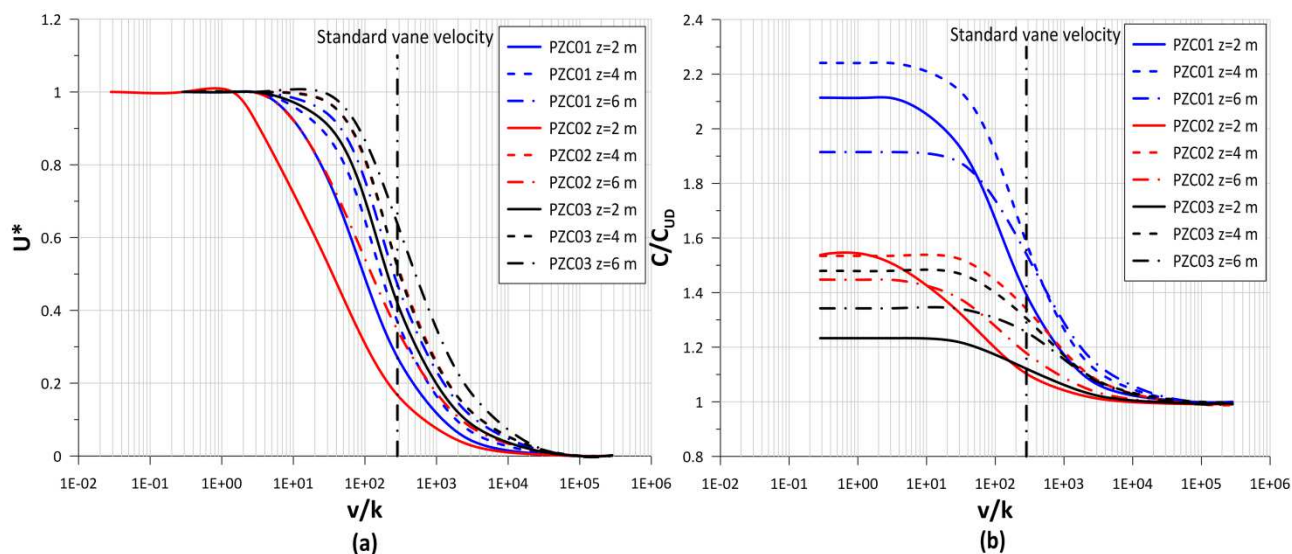
counterpart.

Figure 10. Numerical results of (a) characteristic drainage curves and (b) normalized torque as a function of zinc mining tailings.

6   Conclusions

The present paper describes the application of a nonlinear poroelastic model to the interpretation of drainage conditions and developed torque during rotational shearing tests under monotonic loading, such as vane tests. The main features of the nonlinear poroelastic model are presented, following by a function for the initial pore pressure distribution in order to better represent the hydraulic boundary conditions involving the problem. It is shown that the model is able to compute the pore pressure dissipation in the medium around a rotating cylinder, making possible to identify the rate effects taking place in intermediate permeability soils.

The model was then validated by results of vane tests in low permeability soils. It can be seen that the trend of increasing resistance with a reduction of the shear rate was captured by the numerical results with reasonable agreement. For the data analyzed, the standard vane rotation rate proved to be suitable to ensure undrained conditions of shearing, as expected in these materials.

A parametrical analysis was conducted varying the main parameters of the poroelastic model, demonstrating that the ratio between drained and undrained torque is mainly affected by the soil resistance, as the stiffness and radius of influence demonstrate little effects in this output.

The model predictions are applied to experimental results of field vane tests in zinc mining tailings, an intermediate permeability material. It has been shown that the standard rate of vane rotation is not suitable to reach undrained conditions in this material, which would require higher velocities depending on the station and depth analyzed. It is concluded that the nonlinear poroelastic model presented shows itself a good tool for evaluating drainage conditions.

Acknowledgments

References

[1] K. Flaate. Factors influencing the results of vane tests. *Canadian Geotechnical Journal*, vol. 3, n. 1, pp. 18-31, 1966.
[2] R. J. Chandler, 1988. The in-situ measurement of the undrained shear strength of clays using the field vane test. In: A. Richards (ed.), *Vane Shear Strength Testing in Soils: Field and Laboratory Studies*, pp. 13-44.
[3] M. Roy and A. Leblanc, 1988. Factors affecting the measurements and interpretation of the vane strength in soft sensitive clays. In: A. Richards (ed.), *Vane Shear Strength Testing in Soils: Field and Laboratory Studies*, pp. 117-128.
[4] J. Bedin. Interpretation of piezocone test in bauxite residues. MSc dissertation, Federal University of Rio Grande do Sul, 2006.
[5] F. Schnaid. *In situ testing in geomechanics – the main tests*. Taylor & Francis, 2009.
[6] E. A. Gauer. Influence of the mini-vane test rotation rate on the strength of a silty soil. MSc dissertation, Federal University of Rio Grande do Sul, 2010.
[7] L. A. Hlenka. A study of rate effects on the prediction of geotechnical parameters of zinc tailings. MSc dissertation, Federal University of Rio Grande do Sul, 2012.
[8] G. Dienstmann. Analysis of in situ tests in transient flow. PhD thesis, Federal University of Rio Grande do Sul, 2015.
[9] E. A. Gauer. Rate effects in vane test. PhD thesis, Federal University of Rio Grande do Sul, 2015.
[10] A. Fayolle. Non-linear elastic analysis of vane test in a transient flow regime. MSc dissertation, Federal University of Rio Grande do Sul, 2016.
[11] G. Dienstmann; F. S. de Almeida; A. Fayolle; F. Schnaid and S. Maghous. A simplified approach to transient flow effects induced by rigid cylinder rotation in a porous medium. *Computers and Geotechnics*, vol. 97, n. 1, pp. 134-157, 2018.
[12] G. E. Blight. A note on field vane testing of silty soils. *Canadian Geotechnical Journal*, vol. 5, n. 3, pp. 142-149, 1968.
[13] M. F. Randolph and S. N. Hope, 2004.. Effect of cone velocity on cone resistance and excess pore pressure. In: *Proceeding of Engineering practice and performance of soft deposits*, pp. 147-152.
[14] O. Coussy. *Poromechanics*. John Wiley & Sons, 2004.
[15] L. Dormieux; D. Kondo and F. J. Ulm. *Microporomechanics*. Joh Wiley & Sons, 2006.
[16] E. Lemarchand; F. J. Ulm and L. Dormieux. The effect of inclusions on the friction coefficient of highly-filled composite materials. *Journal of Engineering Mechanics*, vol. 128, n. 8, pp. 876-884.
[17] S. Maghous; L. Dormieux and J. F. Barthélémy. Micromechanical approach to the strength properties of frictional geomaterials. *European Journal of Mechanics*, vol. 28, n. 1, pp. 179-188.
[18] K. Y. Lo and A. G. Stermac, 1965. Induced pore pressures during pile-driving operations. In: *Proceedings of the 6th International Conference on Soil Mechanics and Foundation Engineering*, pp. 285-289.
[19] P. H. Morris and D. J. Williams. A revision of Blight's model of field vane testing. *Canadian Geotechnical Journal*, vol. 43, n. 9, pp. 928-948, 2000.
[20] M. F. Randolph and C. P. Wroth. An analytical solution for the consolidation around a driven pile. *International Journal for Numerical and Analytical Methods in Geomechanics*, vol. 3, n. 1, pp. 217-229, 1979.
[21] J. C. Chai; H. M. D. Julfikar; J. Carter and S. L. Shen. Cone penetration-induced pore pressure distribution and dissipation. *Computers and Geotechnics*, vol. 57, n. 1, pp. 105-113, 2014.
[22] A. S. Vésic. Expansion of cavities in infinite soil mass. *Journal of the Soil Mechanics and Foundations Division*, vol. 98, n. 3, pp. 265-290, 1972.
[23] M. Perlow and A. F. Richards. Influence of shear velocity on vane shear strength. *Journal of Geotechnical Engineering*, vol. 103, n. 1, pp. 19-32, 1977.
[24] B. A. Torstensson, 1977. Time-dependent effects in the field vane test. In: *Symposion on soft clay*, pp. 387-397.
[25] G. Biscontin and J. Pestana. Influence on peripherical velocity on vane shear strength of an artificial clay. *Geotechnical Testing Journal*, vol. 24, n. 4, pp. 423-431, 2001.
[26] B. F. Schlue; T. Moerz and S. Kreiter. Influence of shear rate on undrained vane shear strength of organic harbor mud. *Journal of Geotechnical and Geoenvironmental Engineering*, vol. 136, n. 1, pp. 1437-1447, 2010.

[27] M. Jamiolkowski; R. Lancellota and D. C. F. Lo Presti, 1995. Remarks on the stiffness at small strains of six Italian clays. In: *Proceedings of Pre-failure Deformation of Geomaterials*, pp. 817-836.
[28] I. Djeran-Maigre and M. Gasc-Bariber. Hydromechanical modeling of experimentally compacted saturated argillaceous porous media. *Transport in Porous Media*, vol. 41, n. 1, pp. 81-103, 2000.